Locally Parity-Time Symmetric and globally Parity-Symmetric systems

W. W. Ahmed[1], R. Herrero[1], M. Botey[1] and K. Staliunas[1,2]
[1]*Departament de Física, Universitat Politècnica de Catalunya (UPC), Colom 11, E-08222 Terrassa, Barcelona, Spain*
[2]*Institució Catalana de Recerca i Estudis Avançats (ICREA), Passeig Lluís Companys 23, E-08010, Barcelona, Spain*

We introduce a new class of systems holding Parity Time (PT)-symmetry locally whereas being globally P-symmetric. The potential is globally symmetric, $U=U(|r|)$, and fulfills PT-symmetry with respect to periodically distributed points r_0: $U(|r_0+r|)=U^*(|r_0-r|)$ being $r_0 \neq 0$. We show that such systems hold novel properties arising from the merging of the two different symmetries, leading to a strong field localization and enhancement at the double-symmetry center, $r=0$, when the coupling of outward to inward propagating waves is favored. We explore such general potentials in 1D and 2D, which could have actual realizations in different fields, in particular in optics, combining gain/loss and index modulations in nanophotonic structures. As a direct application, we show how to render a broad aperture VCSEL into a bright and narrow beam source.

PACS numbers: 78.20.Bh, 42.79.- e, 85.60.-q, 42.25.Bs

PT-symmetric systems, introduced as a curiosity in quantum mechanics [1,2], are recently being explored in the field of optics, acoustics, plasmonics or Bose-Einstein condensates [3-8]. A necessary condition for a system to be PT-symmetric is that the complex potential fulfills $U(r)=U^*(-r)$. Such complex systems with real spectra may support novel unexpected properties[9-11].

Most PT-symmetric systems can be regarded as belonging to two limiting situations of complex periodic potentials. On one extreme, there are purely real-valued potentials holding real periodic modulations in space; which potential, in the simplest harmonic modulation case, reads: $U(r) = n_{\mathrm{Re}} \cos(qx)$, being q the spatial period of the modulation and n_{Re} its amplitude. On the other extreme, we find purely imaginary potentials only exhibiting gain-loss modulations, which in the simplest harmonic case may be expressed as: $U(r) = n_{\mathrm{Im}} \cos(qx)$. Both limits lead to a symmetric coupling of resonant modes, i.e. the two counter-propagating modes with wavevector $|k|$, $\exp(-ikx)$ and $\exp(ikx)$, are coupled symmetrically at resonance, for $q = 2k$. The most peculiar situation arises when both the real and imaginary parts of the potential are simultaneously modulated, with a $\pm\pi/2$ phase shift: $U(r) = n_{\mathrm{Re}} \cos(qx) + n_{\mathrm{Im}} \sin(qx)$. When both modulations are balanced, $n_{\mathrm{Re}} = n_{\mathrm{Im}}$, the complex potential can be simply expressed as: $U(r) = n \exp(\pm iqx)$, which evidences that the coupling becomes strongly unidirectional. E.g. for such a complex modulation the left-propagating mode $\exp(-ikx)$, is efficiently coupled to the right propagating mode, $\exp(+ikx)$, but not vice versa. The point $n_{\mathrm{Re}} = n_{\mathrm{Im}}$ is precisely the so-called phase transition, separating two extreme situations. Mathematically, the coupling between left/right propagating modes is conveniently described via linear coupling matrices, $M = \{\{0, n_{\mathrm{Re}}+n_{\mathrm{Im}}\}, \{n_{\mathrm{Re}}-n_{\mathrm{Im}}, 0\}\}$ which at the PT-phase transition point degenerate to $M = \{\{0,2n\},\{0,0\}\}$. Generally, in the presence of several modes (or mode continuum) the situation becomes more engaged, however the phase transition separating the two extreme limits of Real-like and purely Imaginary-like potentials still exists. The question that arises is what occurs if the PT-symmetry condition is not met globally but only locally. Let us consider a simple one-dimensional (1D) situation as the one represented on Fig.1a: such a complex potential leads to a unidirectional coupling "to the left" on the right half-space, and "to the right" on the right half-space. Therefore, an accumulation of the field can be expected at $x = 0$. The same idea applies to 2D (see Fig.1b and Fig.1d), when the radial coupling between incoming and outgoing axisymmetric waves is asymmetric. Note that the physical realizations of the two above discussed arrangements, in 1D and 2D, are nowadays available in microphotonics, in particular by special microfabrication techniques of microchip- and VCSEL lasers [12-14]. In optics, the refractive index corresponds to the real component of the potential whereas gain/loss stands for its imaginary part. Purely real or imaginary modulated systems being Photonic Crystals and Gain/Loss Modulated (GLM) systems, respectively [15-18]. Therefore,

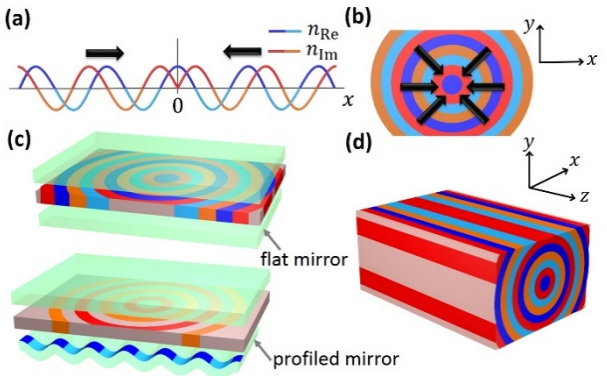

PT-symmetric optical potentials are expected to behave either as PhC-like systems or as GLM-like systems.

FIG. 1. (color online) Inwards unidirectional coupling: (a) 1D complex potential, where n_{Re} and n_{Im} correspond to the real and imaginary parts of the modulation of the potential; (b) analogous axisymmetric configuration in 2D. (c) Two possible realizations of such 2D geometries in broad aperture microlasers (modified VCSELS) with either a modulated gain-layer and/or a modulated (micro-corrugated) mirror, with asymmetric spatial coupling of the fields evolving in time. (d) 3D coaxial complex modulation, analogous to (b) and (c), with asymmetric radial coupling for fields propagating along z. The arrows in (a) and (b) indicate the direction of the asymmetric mode coupling.

In this article, we propose a novel class of locally PT-symmetric and globally P-symmetric for field localization and enhancement, which we analyze on general linear systems both in 1D and in 2D, to finally explore the dynamics of a 2D VCSEL, represented by a nonlinear model with such a

potential, to show the universality and applicability of the proposal.

We start by the general paraxial electromagnetic field equation (equivalent to the Schrödinger equation for a quantum wave-function) as a mathematical model, including diffraction and a complex potential, as:

$$\partial_t A(r,t) = i\nabla_\perp^2 A(r,t) + iU(r)A(r,t) \qquad (1)$$

where $A(r,t)$ is the slowly varying amplitude envelope of the complex electromagnetic field distributed in space, r, and $U(r)$ is the potential with a profile satisfying the particular symmetry conditions. The particular requirement for the potential is the local PT-symmetry: $U(|r_0+r|) = U^*(|r_0-r|)$, for periodically distributed points r_0, $r_0 \neq 0$; and the global P-symmetry: $U(r) = U(-r)$ for all r. For simplicity, using normalized spatial coordinates, such a potential may be expressed as: $U(r) = n_{\mathrm{Re}}\cos(|x|+\phi) - in_{\mathrm{Im}}\sin(|x|+\phi)$ in 1D, and $U(r) = n_{\mathrm{Re}}\cos(r+\phi) - in_{\mathrm{Im}}\sin(r+\phi)$ in 2D. Here, n_{Re} and n_{Im} denote the normalized amplitudes of the real and the imaginary component of the potential, respectively. The phase, ϕ, characterizes the P-symmetry center, at $r=0$, and it is a crucial parameter for the field localization and enhancement. Therefore, n_{Re}, n_{Im} and ϕ are the three key parameters determining the spatial and temporal dynamics of such systems. Equation (1) describes the field temporal evolution of the schemes represented in Figs. 1a-1c, or equivalently, the spatial evolution for propagation along z for Fig. 1d.

We numerically solve Eq. (1) considering the general 1D potential $U(r) = n_{\mathrm{Re}}\cos(|x|+\phi) - in_{\mathrm{Im}}\sin(|x|+\phi)$, for an initial Gaussian beam: $A(x) = A_0 e^{(-x/w)^2}$ where the initial beam width w is broad enough to see the modulation ($w >> 1$). As expected, such a system develops an exponential field localization at $x=0$, also exhibiting an exponential growth in time for most of the parameter sets, due to the linear nature of the system. The envelope of the field may be asymptotically expressed as: $A(x) \approx e^{i\omega t} e^{ik|x|}$ where $k = k_{\mathrm{Re}} + ik_{Im}$ and $\omega = \omega_{\mathrm{Re}} + i\omega_{Im}$ are both complex functions; k_{Im} and k_{Re} denote the spatial localization exponent and wavenumber of a dominant mode, respectively, while ω_{Im}, ω_{Re} stand for the temporal growth exponent and temporal oscillation frequency. We numerically obtain the localization as: $k_{Im} = d/dt(\log A(x,t))$, after a sufficient long evolution time; and the temporal growth at $x=0$ as: $\omega_{Im} = d/dt(\log A(0,t))$. We explore the parameter space $(n_{\mathrm{Re}}, n_{\mathrm{Im}})$ to determine the regimes of maximum field localization and growth, the results are summarized in Fig. 2.

The field is expected to be localized around the *P*-symmetry point for $n_{\mathrm{Re}} \approx n_{\mathrm{Im}}$, resulting from the unidirectional coupling between propagating waves, on the left-hand $x<0$ and right-hand $x>0$ half-spaces. The dark blue area in both maps represents almost no localization (Fig.2a) or no field growth (Fig.2b). We observe that the growth for $\phi = 0$ is larger at the top and bottom regions, see Fig. 2b, suggesting that it strongly depends on the amplitude of gain modulation, n_{Im}. More precisely, the growth attains large values for parameter sets with $|n_{\mathrm{Im}}| > |n_{\mathrm{Re}}|$ where the system displays a GLM-like behavior. However, on the top-right quadrant $(n_{\mathrm{Re}} > 0, n_{\mathrm{Im}} > 0)$, for $\phi = 0$, the P-symmetry and the presence of a higher index at $x=0$ surrounded by gain areas, leads to large growths and strong localizations for large values of n_{Im} and n_{Re} values, indicating the crucial role of the interplay between the real and the imaginary modulations, Fig. 2a.

To illustrate the effect of the PT-potential on the spatio-temporal field dynamics, we consider two representative points, (c) and (d), with the same gain/loss modulation but opposite sign in the index modulation profile, laying within and outside the field localization area. Note that while for point (c) the potential leads to an inwards coupling of the wavevectors inducing a sharp field localization, see Fig. 2c(i), the coupling at point (d) is outwards and the field is spatially spread, see Fig. 2d(i). The same field profiles represented in logarithmic scale evidence the exponential character of the localization in Fig. 2c(ii) while localization is nearly zero for the flat curve of Fig. 2d(ii). We also provide both spatial field spectra in Fig. 2c/d(iii) as obtained from the Fourier transform, although resonant peaks are not visible for point (c) due to the exponential slopes. Note that the spectrum in Fig. 2c(iii) extends over the first and second harmonics of the modulation. The effect of index and gain modulation on field localization and enhancement, for $\phi = 0$, in parameter space, is also shown in Supplementary video 1.

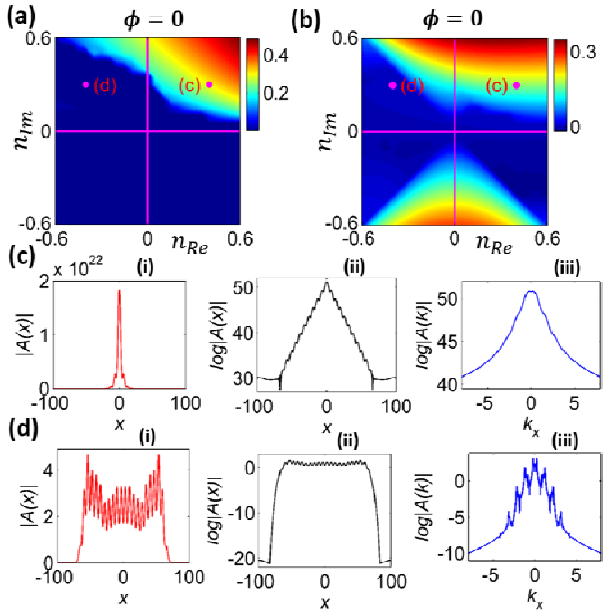

FIG. 2. (color online) (a) Localization (k_{Im}) map calculated after a sufficient long time (t~300 units) in parameter space (n_{Re}, n_{Im}) for $\phi = 0$. (b) Growth (ω_{Im}) map at the center ($x=0$) for $\phi = 0$ in the parameter space, obtained numerically with finite difference time domain method using an hypergaussian filter as boundary conditions. (c,d) Analysis of two representative points, with parameter sets (0.4,0.3) and (-0.4,0.3),

respectively. For both points, the spatial field profiles in linear and logarithmic scales are shown in (i) and (ii), while (iii) represents the spatial field spectra, as obtained from the Fourier transform, in logarithmic scale.

The localization is, however, remarkably phase dependent, occurring in different quadrants of the parameter space for different phases. Figures 3a, 3b and 3c provide the localization maps for the representative phases: π/4, π /2 and π. Note that, while for ϕ = π/4 localization also occurs for $(n_{\mathrm{Re}} > 0, n_{\mathrm{Im}} > 0)$, a comparison with the map provided in Fig. 2b clearly indicates that the most intense field localization is achieved for $\phi = 0$.

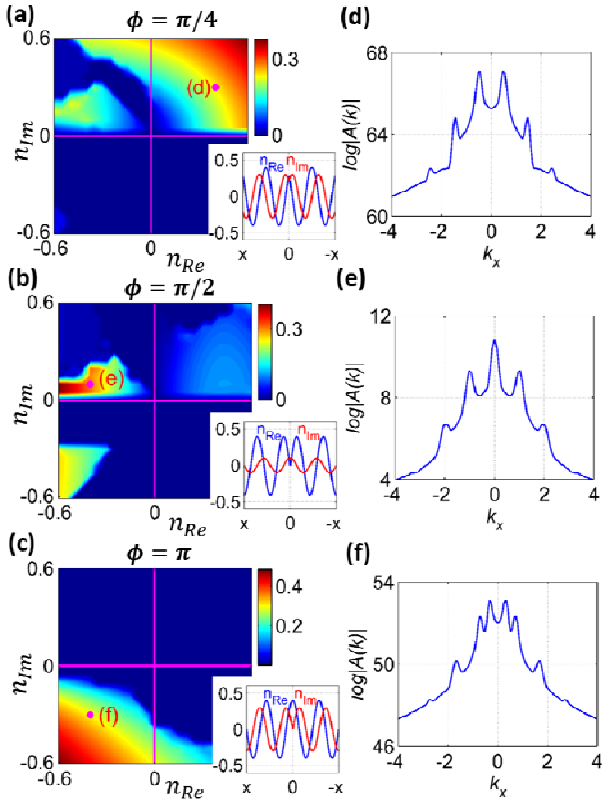

FIG. 3. (color online) (a,b,c) Localization maps calculated after a sufficient long time (t~300 units) in parameter space (n_{Re}, n_{Im}) for: ϕ =π/4, π/2 and π, respectively. (d,e,f) Spatial field spectrum as obtained from the Laplace transform, in logarithmic scale, for representative points within the field localization areas for each phase. The dominant modes of representative points. In (d) the dominant modes are k_x= 0, 0.5, 2.5,... in (e) the dominant modes are k_x = 0,1,2.. ; and in (f) are k_x ~0.3, ~0.7, ~1.70, ...

For ϕ = π/2 strong localization flips to the second quadrant $(n_{\mathrm{Re}} < 0, n_{\mathrm{Im}} > 0)$ where the system is almost PhC-like. Further increasing the phase, for ϕ = π, localization moves on to the third quadrant $(n_{\mathrm{Re}} < 0, n_{\mathrm{Im}} < 0)$ (being the corresponding map exactly symmetric to the one for ϕ = 0). The Supplementary video 2 visualizes how the localizations regime spins counterclockwise when then phase increases. Localization is stronger when the asymmetric coupling between wavevectors provided by the local PT-symmetric complex optical potential is directed inwards, see the insets of Figs. 3a and 3c, being enhanced for larger gain/loss modulation amplitudes, these situations correspond to a GLM-like regimes. Note that strong localization is achieved around $x = 0$ due to combined effect of local PT- and global P-symmetry. However, standalone P-symmetry can also provide some localization for particular phases, e.g; localization at the $n_{\mathrm{Re}} = 0$ axis in Fig. 3a. In addition, a small localization region, is also found for ϕ = π/2, clearly indicating it is a PhC-like behavior, not relaying on the coupling, which is outwards in the case of Fig. 3b.

A direct interpretation of the different localization regimes may be based on the competition of spatial modes in the field spectra. The interaction of different growing modes gives birth to different localization regimes, depending upon the modulation amplitudes and phase. Since the spatial modes have an intrinsic complex nature: $k = k_{\mathrm{Re}} + ik_{Im}$, the commonly used Fourier transform does not allow a precise localization of the real components of the spectrum, as growing modes have exponential slopes. In this situation, the Laplace transform is the optimal method to explore the complex spectrum [19]. The Laplace transform defined as: $A(s) = \int_0^\infty A(x)e^{-sx}dx$ is a generalization of the Fourier transform, since being $s = \sigma + ik$ it reduces to the Fourier transform for $\sigma = 0$. For a decaying field in the form: $A(x) = e^{-(ik_{\mathrm{Re}} - k_{\mathrm{Im}})x}$, the Fourier and Laplace transforms result respectively as : $A(k) = 1/[k_{\mathrm{Im}} + i(k_{\mathrm{Re}} - k)]$ and $A(s = \sigma + ik) = 1/[(k_{\mathrm{Im}} - \sigma) + i(k_{\mathrm{Re}} - k)]$. This Laplace transform has a pole at $(\sigma, k) = (k_{\mathrm{Im}}, k_{\mathrm{Re}})$ and the cross-section over the pole $\sigma = k_{\mathrm{Im}}$ gives a sharp peak. We obtain the Laplace transform numerically, which however is defined on the half plane, $k_{\mathrm{Im}} \geq \sigma$ and provide its cross-section for $k_{\mathrm{Im}} \approx \sigma$, where σ is calculated from the field localization exponent in Figs. 3d, 3e and 3f for particular parameter sets. We essentially identify three distinct regimes on the basis of symmetric spatial modes participating in the field spectrum. The simplest case corresponds to the PhC-like limit, where a set of dominant integer modes k_x =0, 1, 2,.. prevail in the spatial spectrum, see Fig. 3b for ϕ = π/2. The other two localization regimes correspond to a GLM-like regime. In a pure GLM system, the spectrum shows frequency peaks centered at 0.5, 1.5, 2.5,... this is the case for ϕ = π/4, see Fig. 3a . However, large gain modulation amplitudes lead to a strong coupling between different harmonics, eventually shifting the central frequency peaks towards lower wavenumbers, e.g. the system dynamics supports the dominant mode set k_x ~0.3, 0.7, 1.7, for ϕ=0, π,... in Fig. 3c.

We proceed to analyze local *PT*-symmetry and global *P*-symmetry in 2D, considering the axisymmetric potential: $U(r) = n_{\mathrm{Re}} \cos(r + \phi) - in_{\mathrm{Im}} \sin(r + \phi)$. The results, for ϕ =0, are summarized in Fig. 4. Analogously to the 1D potential, a field enhancement is found at the center, $r = 0$, now attributed to the asymmetric radial coupling between inward and outward propagating waves. Figure 4a provides the localization obtained from the correspondingly linearized field. Since the axial cross-sectional profile of the field, see Fig. 4 c(v), is not exponentially

decreasing, due to the $1/r$ factor of the axial symmetry, localization is obtained from the exponential slope of $A(r)\cdot\sqrt{r}$, see Fig. 4c(vi). The top right side of the map, $(n_{\mathrm{Re}}>0, n_{\mathrm{Im}}>0)$, exhibits the highest localization area, approximately corresponding to the one obtained in 1D in Fig. 2b. This result, along with the central growth map for $r = 0$, provided in Fig. 4b indicates that the overall scenario resembles the 1D situation. The field profile shows a sharp peak in the 2D plane for the parameter set of point (c) laying within the localization range, see Figs. 4c(i) and (iv). Additionally, Figs. 4c(iii) and (vii) depict the phase of the field in which slope increases with jumps from $-\pi$ to $+\pi$, clearly showing the inwards propagation. Tough, while remaining analogous to 1D the proposed effect in this 2D case is more realistic and opens new avenues in optics for extraordinary field confinement and high power density at a selected position. Next, we provide an example to demonstrate the functionality of our proposal in a nonlinear regime.

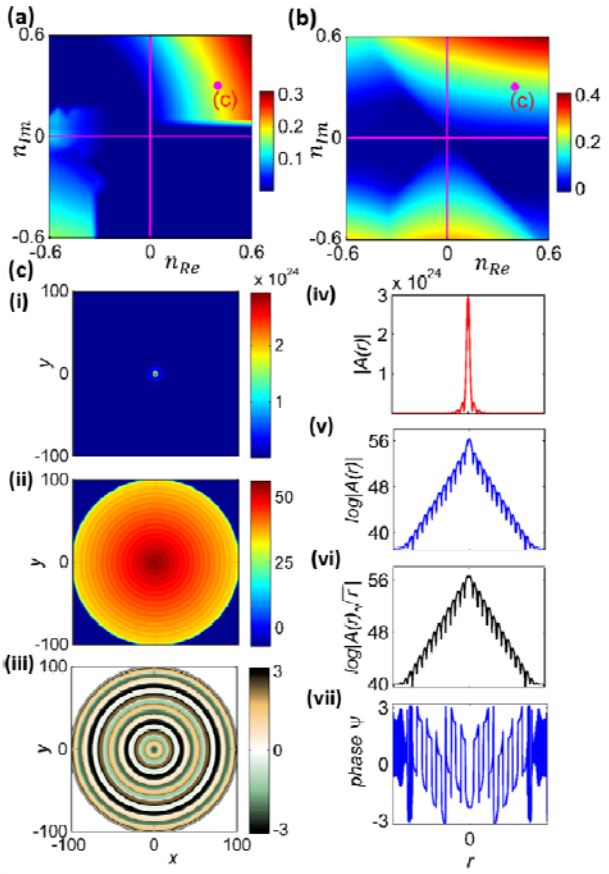

FIG. 4. (color online) (a) Localization (k_{Im}) map of the axial cross-section profile of the field linearized as: $A(r)\cdot\sqrt{r}$ for a 2D local PT-axisymmetric and global P-axisymmetric as in Fig. 1b, calculated after sufficient long time (t~300 units) in parameter space (n_{Re} , n_{Im}). (b) Growth (ω_{Im}) map of at the center ($r = 0$) in parameter space. A strong field enhancement and localization at $r = 0$ is shown in (c) for the parameter set (0.4, 0.3). (i,ii) 2D spatial field profiles in linear and logarithmic scales, respectively. (iii) Field phase. Panels (iv),(v),(vii) display the axial cross-sectional profiles of (i)-(iii), whilst (vi) depicts the linearized field, $A(r)\cdot\sqrt{r}$, in logarithmic scale.

Broad aperture lasers, and VCSELs among them, are relevant laser sources however suffering from a major drawback a poor beam quality due to the lack of an intrinsic transverse mode selection mechanism. In lowest approximation, the field dynamics of VCSELS with the proposed complex potential profile, $U(r)$, satisfying the particular proposed conditions in either 1D and 2D axisymmetric conditions, can be described by complex Ginzburg-Landau equation [20]:

$$\partial_t A(r,t) = (p - |A|^2)A + i\nabla_\perp^2 A(r,t) + iU(r)A(r,t) \qquad (2)$$

where $A(r,t)$ is the envelope of complex field distributed in space, r, and p is pump parameter. The nonlinearity is due to gain saturation. The complex potential profile, $U(r)$, satisfies the local PT-symmetry and global P-symmetry conditions for 1D and 2D axisymmetric conditions as discussed above. Such nonlinear systems generally show the saturation phenomena with uniform field distribution for $p > 0$. However, the field localization and enhancement in such situation is possible at the center for $p < 0$ by applying locally PT-symmetric and globally P-symmetric potential. The results for a particular parameter set are provided in Fig. 5. The spatial field profile showing the concentration at the center, $r = 0$, in Fig. 5a, reveals that this 2D axisymmetric system efficiently localizes the field.

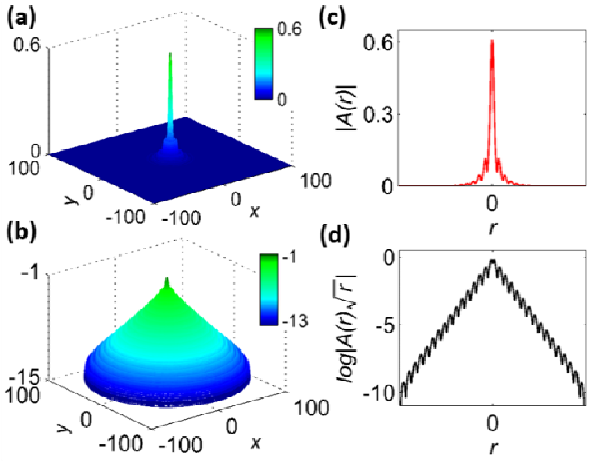

FIG. 5. (color online) Spatial field distributions for a 2D locally PT- symmetric and globally P-symmetric VCSEL, calculated after the steady state (t~150 units) for $p = -0.1$ and parameter set (0.4, 0.4). 3D visualization of the VCSEL output field profile, concentrated and enhanced at $r = 0$ in real (a) and logarithmic (b) scales. (c)/(d) Axial cross-sectional profile the field in linear/logarithmic scale.

To conclude, we propose a novel class of local PT-symmetric and global *P*-symmetric systems providing a unique platform for extreme field localization and enhancement around the P-symmetry point. Such systems have the capability to simultaneously localize and enhance the field due to the asymmetric radial coupling of inward and outward waves. Specifically, this new systems can strongly localize the field, depending on the relative modulation amplitudes and phase of the complex potential. Therefore, the most interesting scenario occurs for GLM-like systems, for which extreme field concentrations are achieved for a wide range of parameter sets, for $\phi = 0$, either in the proposed 1D and 2D axisymmetric configurations. Also for PhC-like systems, less significant field localizations are obtained for some particular potential phases.

The fundamental concept may also be easily implemented to

find remarkable applications in various linear and nonlinear optoelectronic devices where a high degree of localization is essentially desirable such as optical switching in nanostructures, optical modulators, or broad aperture lasers and microlasers. In particular, we show a possible direct application for an axially modulated 2D VCSEL to improve the brightness and quality of beam emission as to show its applicability in particular implementation. We want to note universality of this nonlinear example as based on a general complex Ginzburg-Landau equation, confirming that the field localization and concentration at around the point of merging of two symmetries and can be realized in other different physical systems in Bose condensates, and acoustics among others.

ACKNOWLEDGEMENTS

We acknowledge financial supported by Spanish Ministerio de Educación y Ciencia and European FEDER (project FIS2011-29734-C02-01). Erasmus Mundus Doctorate Program Europhotonics (Grant No. 159224-1-2009- 1-FR-ERA MUNDUS-EMJD) supported the work of W.W.A.

References:

[1] C. M. Bender and S. Boettcher, Phys. Rev. Lett. **80**, 5243 (1998).
[2] C. M. Bender, Rep. Prog. Phys. **70**, 947 (2007).
[3] A. Guo, G. J. Salamo, D. Duchesne, R. Morandotti, M. Volatier-Ravat, V. Aimez, G. A. Siviloglou, and D. N. Christodoulides, Phys. Rev. Lett. **103**, 093902 (2009).
[4] C. E. Ruter, K. G. Makris, R. El-Ganainy, D. N. Christodoulides, M. Segev, and D. Kip, Nat. Phys. **6**, 192 (2010).
[5] A. Regensburger, C. Bersch, M. A. Miri, G. Onishchukov, D. N. Christodoulides and U. Peschel, Nature, **488**, 167 (2012).
[6] X. Zhu, H. Ramezani, C. Shi, J. Zhu, and X. Zhang, Phys. Rev. X **4**, 031042 (2014).
[7] H. Benisty, A. Degiron, A. Lupu, A. De Lustrac, S. Che´nais, S. Forget, M. Besbes, G. Barbillon, A. Bruyant, S. Blaize, and G. Le´rondel, Opt. Express **19**, 18004 (2011)
[8] D. Haag, D. Dast, H. Cartarius, and G. Wunner, Phys. Rev. A **92**, 053627 (2015)
[9] S. Longhi, J. Phys. A, Math. Theor. **44**, 485302 (2011).
[10] Z. Lin, H. Ramezani, T. Eichelkraut, T. Kottos, H. Cao, and D. N. Christodoulides, Phys. Rev. Lett. **106**, 213901 (2011)
[11] L. Feng, Y.-L. Xu, W. S. Fegadolli, M.-H. Lu, J. E. Oliveira, V. R. Almeida, Y.-F. Chen, and A. Scherer, Nat. Mater. **12**, 108 (2012).
[12] K. Hirose, Y. Liang, Y. Kurosaka, A. Watanabe, T. Sugiyama, and S. Noda, Nat. Photonics, **8**, 406 (2014).
[13] H. Hodaei, M. A. Miri, M. Heinrich, D.N. Christodoulides, and M. Khajavikhan, Science, **346**, 975 (2014).
[14] K. Iga, IEEE J. Sel. Top. Quantum Electron. **6**, 1201 (2000).
[15] K. Staliunas, R. Herrero, and R. Vilaseca, Phys. Rev. A **80**, 013821 (2009).
[16] M. Botey, R. Herrero, and K. Staliunas, Phys. Rev. A **82**, 013828 (2010).
[17] R. Herrero, M. Botey, M. Radziunas, and K. Staliunas, Opt. Lett. **37**, 5253, (2012).
[18] M. Radziunas, M. Botey R. Herrero, and K. Staliunas, Appl. Phys. Lett. **103**, 132101 (2013).
[19] P. Moreno and A. Ramirez, IEEE Trans. Power Delivery, **23**, 2599 (2008).
[20] W. W. Ahmed, S. Kumar, R. Herrero, M. Botey, M. Radziunas, and K. Staliunas, Phys. Rev. A, **92**, 043829 (2015).